Laser-ultrasonic measurements of residual stresses on aluminum 7075 surface-treated by low plasticity burnishing
Moreau, A.; Man, C.-S.

National Research Council Canada   Conseil national de recherches Canada

Canada

Laser-Ultrasonic Measurements of Residual Stresses on Aluminum 7075 Surface-Treated by Low Plasticity Burnishing

A. Moreau[1] and C.-S. Man[2]

[1] National Research Council of Canada, Industrial Materials Institute, 75 de Mortagne, Boucherville, QC J4B 6Y4
[2] Department of Mathematics, University of Kentucky, 715 Patterson Office Tower, Lexington, KY 40506-0027

Abstract

A convenient non-destructive means of characterizing residual stresses would be highly desirable. Ultrasonics is one of very few techniques which might succeed at this. However, the effects of residual stresses on ultrasound propagation are small and can be hidden by other material properties, especially crystallographic texture. The traditional ultrasonic approach has been to compare the surface before and after surface processing, assuming that texture remains unchanged. However, surface processing does affect surface texture and the traditional approach often fails. In this paper, we present a novel method to measure surface residual stresses with ultrasound when the process also modifies surface texture. Then, we apply this method to a sample of aluminum 7075-T651 surface treated using low-plasticity burnishing (LPB). This technique can produce a very smooth surface, a stress gradient that penetrates relatively deeply into the material, and an anisotropy of the residual stresses. The velocity of surface acoustic waves (Rayleigh waves and surface skimming longitudinal waves) was measured as a function of propagation direction and frequency on as-received and LPB-treated surfaces. The observed differences are used to estimate the magnitudes and directions of the two principal components of the residual stresses induced by the LPB process, independently of surface texture modifications.

Introduction

Low-plasticity burnishing (LPB) is an emerging surface processing technique used to introduce deep compressive surface residual stresses that improve the durability of parts. With this technique, a ball or a roll applies pressure to the surface and compressive surface residual stresses are produced. These stresses vary in magnitude with depth and they may also be anisotropic. Non-destructive measurements of residual stresses, their anisotropy, and their distribution as a function of depth, imparted by the LPB process and other surface processing techniques are being sought by various groups to verify process quality and residual stress retention over time.

Residual stress measurement techniques such as x-ray diffraction or the hole drilling technique almost always destroy or damage the part being measured. Non-destructive techniques are essentially limited to ultrasonic, eddy current, and magnetic techniques. The magnetic technique is applicable only to ferromagnetic materials and it depends on many microstructural parameters other than residual stresses. Consequently, its results are difficult to interpret. Eddy current techniques have shown promise for Ni based alloys, but the technique is under development and may not be applicable to other types of alloys [1]. However, most non-destructive characterization work has been done with ultrasonics because ultrasonic characterization is inexpensive and flexible. Moreover, surface acoustic waves have the potential of providing a depth profile of the residual stresses by varying the ultrasonic frequency. In

addition, recent developments in laser-ultrasonic technology, a technology to generate and detect ultrasound with laser light, bring additional advantages: non-contact measurement that works on hot or moving parts, flexibility in source and detection geometry, wide bandwidth.

Ultrasonic methods are based on measuring ultrasound velocity changes caused by internal stresses. These stresses can be externally applied or internal to the part. A typical measurement procedure is as follows: A reference sample is made for calibration purposes. A stress smaller than the yield stress is applied to the reference sample and one measures the change in ultrasound velocity with applied stress. This change is usually linear and the slope of the velocity change with applied stress is called the acoustoelastic constant. The measurement can be repeated with various ultrasonic waves (compression waves, shear waves, surface waves) in various directions, leading to various acoustoelastic constants. For example, for aluminum, the relative change on compression wave velocity in the direction of tensile strength is approximately -5.2×10^{-5}/MPa. When the wave is travelling in the direction perpendicular to the applied stress, the acoustoelastic constant is $+0.84 \times 10^{-5}$/MPa. For an applied stress of 100 MPa, this corresponds to a +0.1 to -0.5% change in velocity. This is small but changes of order 0.01% can be measured routinely when following adequate procedures. To insure that chemistry, microstructure, or any processing step does not affect the sound velocity also, differential measurements are made. Either the reference sample is closely matched to the part to be measured or, usually, one measures the change in ultrasound velocity caused by the process utilized to impart a residual stress.

The main difficulty with ultrasonics is that crystallographic orientation distribution, i.e. texture, affects the ultrasound velocity considerably more than residual stresses. For example, the compression sound velocity can vary by up to 3% between the ideal 100 and 111 texture of aluminum, and by 15% in iron. Processes used to apply compressive surface stresses do affect surface texture somewhat and this is a major source of difficulty. In this paper, a simplified model of the dependence of ultrasound velocity on texture and residual stresses will be adopted. This model will allow us to design a measurement procedure that can decouple the two contributions. Then we will present laser-ultrasonic measurements on a sample of aluminum alloy 7075-T651. These measurements involve the propagation of two acoustic modes (surface acoustic waves, and surface skimming compression wave) as a function of propagation direction and frequency on the as-received and LPB-treated surfaces. These data are utilized to estimate the principal components and directions of residual stresses induced by the LPB process.

Ultrasound velocity theory

In this paper, a simplified yet practical and reasonably accurate model for the acoustoelastic response of weakly-textured polycrystalline aggregates is used to describe the dependence of ultrasound on texture and residual stresses. This simplified model is a special case of a more general model based on Hartig's law [2] and linear elasticity with initial stress [3], where the incremental (second Piola-Kirchhoff) stress is taken as the sum of two terms, one being the image of the fourth order elasticity tensor C, and the other that of the sixth order acoustoelastic tensor D. Here it will be assumed that the anisotropic part of C is linear in the texture coefficients and D is an isotropic tensor function bilinear in the initial stress and the infinitesimal strain with respect to the initial configuration (i.e., the effect of crystallographic texture on D is ignored). It follows that D is defined by four material parameters $\beta_1, \beta_2, \beta_3, \beta_4$, and C generally carries five elastic constants. For aggregates of cubic crystallites, however, the number of elastic constants that appear in C reduces to three, which we denote by λ, μ, and α. In what follows, for the aluminum sample in question, we use the HM-V_c model [4] and the Man-Paroni model [5,6] to compute the values of the aforementioned material parameters from single-crystal second-order [7] and third-order [8] elastic constants for C and D, respectively. The results are: $\lambda = 58.43\,\text{GPa}$, $\mu = 26.15\,\text{GPa}$, $\alpha = -16.83\,\text{GPa}$, $\beta_1 = 0.89$, $\beta_2 = 0.96$, $\beta_3 = -2.63$, and $\beta_4 = -4.54$.

Under this setting, the shift of velocity from its value pertaining to isotropic texture and no initial stress can de decomposed into two parts: one caused by crystallographic texture (the ODF) and one caused by

initial or residual stresses. Interaction between these two terms is neglected. In this paper we further assume that the texture of the sample in question has orthorhombic symmetry. The simplified model can be used to calculate the velocity of any ultrasonic wave but this paper makes use only of the surface skimming compressional waves, also called P waves, and of Rayleigh surface waves. These waves propagate on or just below the surface and their velocities depend on the propagation direction θ with respect to some reference direction. Let the normal direction to the free surface be the 3-axis, and the reference direction in the plane of the surface (this might be the rolling direction) be the 1-axis. Let the symmetry axes of the orthorhombic texture be labeled by 1', 2', and 3'. We assume that the 3'-axis is normal to the free surface of the sample. Within these specifications, the model predictions of the Rayleigh wave velocity, V_R, and of the P wave velocity, V_P, are:

$$\frac{V_R - V_{R0}}{V_{R0}} = \begin{aligned}[t] &0.610\,W_{400} - 1.143\,W_{420}\cos2(\theta - \theta_W) - 0.177\,W_{440}\cos4(\theta - \theta_W) \\ &- 0.44\times10^{-5}\,T_m + 2.26\times10^{-5}\,T_d\cos2(\theta - \theta_{RS}) \end{aligned} \tag{1}$$

$$\frac{V_P - V_{P0}}{V_{P0}} = \begin{aligned}[t] &-0.228\,W_{400} + 0.481\,W_{420}\cos2(\theta - \theta_W) - 0.636\,W_{440}\cos4(\theta - \theta_W) \\ &- 4.35\times10^{-5}\,T_m + 6.02\times10^{-5}\,T_d\cos2(\theta - \theta_{RS}) \end{aligned} \tag{2}$$

where the subscripts $R0$ and $P0$ refer to the velocities in a material with isotropic texture and no residual stresses, θ is the angle between the propagation direction and the 1-axis, θ_W is the angle between the 1'-axis and the 1-axis, σ_a and σ_b are the principal stresses in the (principal) a- and b-direction, respectively, θ_{RS} is the angle between the a-direction and the 1-axis, $T_m = (\sigma_b + \sigma_a)/2$, $T_d = (\sigma_b - \sigma_a)/2$, and the stresses are in units of MPa. The W_{4m0} coefficients are the fourth-order crystallographic orientation distribution coefficients (ODCs) that are obtained from the ODF when it is expressed as a series expansion in Roe's notation [9]. Roe's notation is used because it is the usual choice in non-destructive evaluation. However, Bunge's notation could also have been used [10]. Except for the numerical constants, the equations would have been the same but W_{400}, W_{420}, and W_{440} would have been replaced by C_4^{11}, C_4^{12}, and C_4^{13}, respectively. One advantage of using the W_{4m0} texture coefficients is that the m index describes the in-plane anisotropy (0, 2 or 4-fold symmetry) and helps give a meaning to the coefficients. This is readily observable from the angular dependence of the velocities in Eqs. (1) and (2).

In most cases, the orthorhombic texture symmetry of the material will align with preferred directions of the manufacturing process. For example, the 1', 2', and 3'-axis directions of the orthorhombic texture symmetry will align with the rolling, transverse, and normal direction of sheet or plate metal. In such cases, it is possible to set $\theta_W = 0$ by choosing the 1, 2, and 3-axis directions to coincide with the appropriate preferred directions of the manufacturing process. However, surface processes such as LPB or shot peening typically produce residual stresses with principal stresses that do not necessarily align with preferred directions of the manufacturing process. Therefore, θ_{RS} is unknown.

The velocities in an ideal isotropic material may be calculated from micromechanical models and the experimental values of pure aluminum, single crystal elastic constants. However, for a number of reasons that are outside the scope of this paper, the calculation often lacks the required accuracy. So in this paper, the isotropic velocities will be treated as unknown values that are nevertheless close to the measured velocities because the right sides of Eqs. (1) and (2) are quantities much smaller than 1.

The model Eqs. (1) and (2) relate the ultrasound velocity to the material's texture and residual stress parameters. The non-destructive evaluation problem is: How can one infer the metallurgical parameters W_{400}, W_{420}, W_{440}, θ_W, T_m, T_d, and θ_{RS} from measurements of ultrasound velocity, V_R and V_P as a function of propagation direction θ? In the context of this paper, we are mostly interested in the last three

parameters describing residual stresses. But, as we shall see shortly, their evaluation requires the evaluation of some of the texture coefficients as well.

Designing an ultrasonic measurement of residual stresses

Eqs. (1) and (2) are recast now by replacing the numerical parameters by Greek letters, with subscripts R and P for the Rayleigh and P waves, respectively. Also, let the surface prior to LPB processing be denoted by a prime, and the same surface after LPB processing be denoted by a double prime. Then:

$$\frac{V'_R - V_{R0}}{V_{R0}} = \alpha_R W'_{400} + \beta_R W'_{420} \cos 2(\theta - \theta'_w) + \gamma_R W'_{440} \cos 4(\theta - \theta'_w) + \delta_R T'_m + \varepsilon_R T'_d \cos 2(\theta - \theta'_{RS}), \quad (3)$$

$$\frac{V''_R - V_{R0}}{V_{R0}} = \alpha_R W''_{400} + \beta_R W''_{420} \cos 2(\theta - \theta''_w) + \gamma_R W''_{440} \cos 4(\theta - \theta''_w) + \delta_R T''_m + \varepsilon_R T''_d \cos 2(\theta - \theta''_{RS}), \quad (4)$$

$$\frac{V'_P - V_{P0}}{V_{P0}} = \alpha_P W'_{400} + \beta_P W'_{420} \cos 2(\theta - \theta'_w) + \gamma_P W'_{440} \cos 4(\theta - \theta'_w) + \delta_P T'_m + \varepsilon_P T'_d \cos 2(\theta - \theta'_{RS}), \quad (5)$$

$$\frac{V''_P - V_{P0}}{V_{P0}} = \alpha_P W''_{400} + \beta_P W''_{420} \cos 2(\theta - \theta''_w) + \gamma_P W''_{440} \cos 4(\theta - \theta''_w) + \delta_P T''_m + \varepsilon_P T''_d \cos 2(\theta - \theta''_{RS}). \quad (6)$$

Without loss of generality, the angles θ'_w, θ''_w, θ'_{RS} and θ''_{RS} are chosen to fall in the range $(-\pi/2, \pi/2)$. Because the isotropic velocities are not known precisely enough to permit an accurate estimate of the left sides of the above equations, we will calculate and measure the difference between the processed and un-processed surfaces. These differences are:

$$\frac{V''_R - V_{R0}}{V_{R0}} - \frac{V'_R - V_{R0}}{V_{R0}} = \frac{V''_R - V'_R}{V_{R0}} = \frac{\Delta V_R}{V_{R0}}, \quad (7)$$

$$\frac{V''_P - V_{P0}}{V_{P0}} - \frac{V'_P - V_{P0}}{V_{P0}} = \frac{V''_P - V'_P}{V_{P0}} = \frac{\Delta V_P}{V_{P0}}. \quad (8)$$

A small error on the isotropic velocities has little impact on $\Delta V_R/V_{R0}$ and $\Delta V_P/V_{P0}$. Each of these quantities is a fractional velocity change as a function of ultrasound propagation angle θ caused by surface processing. Because the measured angle is θ, and not its difference with some yet unknown reference angle θ_w or θ_{RS}, it is useful to isolate the θ dependence. To do this, Eqs. (7-8) are rewritten as:

$$\Delta V_R / V_{R0} = A_R + B_R \cos 2\theta + C_R \sin 2\theta + D_R \cos 4\theta + E_R \sin 4\theta, \quad (9)$$

$$\Delta V_P / V_{P0} = A_P + B_P \cos 2\theta + C_P \sin 2\theta + D_P \cos 4\theta + E_P \sin 4\theta, \quad (10)$$

where

$$\begin{aligned}
A_R &= \alpha_R (W''_{400} - W'_{400}) + \delta_R (T''_m - T'_m) \\
B_R &= \beta_R (W''_{420} \cos 2\theta''_w - W'_{420} \cos 2\theta'_w) + \varepsilon_R (T''_d \cos 2\theta''_{RS} - T'_d \cos 2\theta'_{RS}) \\
C_R &= \beta_R (W''_{420} \sin 2\theta''_w - W'_{420} \sin 2\theta'_w) + \varepsilon_R (T''_d \sin 2\theta''_{RS} - T'_d \sin 2\theta'_{RS}), \qquad (11) \\
D_R &= \gamma_R (W''_{440} \cos 4\theta''_w - W'_{440} \cos 4\theta'_w) \\
E_R &= \gamma_R (W''_{440} \sin 4\theta''_w - W'_{440} \sin 4\theta'_w)
\end{aligned}$$

$$A_P = \alpha_P(W''_{400} - W'_{400}) + \delta_P(T''_m - T'_m)$$

$$B_P = \beta_P(W''_{420}\cos 2\theta''_W - W'_{420}\cos 2\theta'_W) + \varepsilon_P(T''_d\cos 2\theta''_{RS} - T'_d\cos 2\theta'_{RS})$$

$$C_P = \beta_P(W''_{420}\sin 2\theta''_W - W'_{420}\sin 2\theta'_W) + \varepsilon_P(T''_d\sin 2\theta''_{RS} - T'_d\sin 2\theta'_{RS}) \quad . \tag{12}$$

$$D_P = \gamma_P(W''_{440}\cos 4\theta''_W - W'_{440}\cos 4\theta'_W)$$

$$E_P = \gamma_P(W''_{440}\sin 4\theta''_W - W'_{440}\sin 4\theta'_W)$$

The parameters A_R to E_R and A_P to E_P can be measured by fitting the ultrasound velocities to the appropriate angular dependence. Eqs. (11-12) are a set of 10 equations with the 14 unknowns: W'_{400}, W'_{420}, W'_{440}, W''_{400}, W''_{420}, W''_{440}, θ'_W, θ''_W, T'_m, T'_d, T''_m, T''_d, θ'_{RS} and θ''_{RS}. Of course, not all of these unknowns can be resolved in terms of the 10 measurable parameters. In fact, the last two of Eqs. (11) and the last two of Eqs. (12) are degenerate and lead to the equalities:

$$D_R\gamma_P = D_P\gamma_R , \tag{13}$$

$$E_R\gamma_P = E_P\gamma_R . \tag{14}$$

These equalities can, in principle, be used to verify the validity of the 4θ dependence of the experimental data but do not provide additional information about the material. However, because $\theta''_W - \theta'_W$ can be close to zero or $\pi/4$, some of these four fitted parameters may be close to zero and Eq. (13) or (14) may be difficult to verify. A better consistency check is obtained by computing

$$\frac{\sqrt{D_R^2 + E_R^2}}{\sqrt{D_P^2 + E_P^2}} = \frac{\gamma_R}{\gamma_P} , \tag{15}$$

which states that the measured magnitude of the 4θ dependence (left side of Eq. (15)) goes as the predicted ratio (right side of Eq. (15)). We are now left with 8 equations in 14 unknowns. Proceeding through the inversion procedure as best as possible, we find:

$$\Delta T_m = T''_m - T'_m = \frac{\alpha_P A_R - \alpha_R A_P}{\alpha_P\delta_R - \alpha_R\delta_P} , \tag{16}$$

$$T''_d\cos 2\theta''_{RS} - T'_d\cos 2\theta'_{RS} = \frac{\beta_R B_P - \beta_P B_R}{\beta_R\varepsilon_P - \beta_P\varepsilon_R} , \tag{17}$$

$$T''_d\sin 2\theta''_{RS} - T'_d\sin 2\theta'_{RS} = \frac{\beta_R C_P - \beta_P C_R}{\beta_R\varepsilon_P - \beta_P\varepsilon_R} , \tag{18}$$

$$\Delta W_{400} = W''_{400} - W'_{400} = \frac{\delta_P A_R - \delta_R A_P}{\alpha_R\delta_P - \alpha_P\delta_R} , \tag{19}$$

$$W''_{420}\cos 2\theta''_W - W'_{420}\cos 2\theta'_W = \frac{\varepsilon_P B_R - \varepsilon_R B_P}{\beta_R\varepsilon_P - \beta_P\varepsilon_R} , \tag{20}$$

$$W''_{420}\sin 2\theta''_W - W'_{420}\sin 2\theta'_W = \frac{\varepsilon_P C_R - \varepsilon_R C_P}{\beta_R\varepsilon_P - \beta_P\varepsilon_R} , \tag{21}$$

$$W''_{440} \cos 4\theta''_w - W'_{440} \cos 4\theta'_w = \frac{D_R}{\gamma_R}, \qquad (22)$$

$$W''_{440} \sin 4\theta''_w - W'_{440} \sin 4\theta'_w = \frac{E_R}{\gamma_R}. \qquad (23)$$

Eqs. (16) and (19) state that the change in the mean residuals stress, ΔT_m, and in the W_{400} texture coefficient, ΔW_{400}, can be obtained from a combination of measurable and known parameters. Eqs. (17-18) describe the change in residual stresses anisotropy. Eqs. (20-23) describe changes in in-plane texture anisotropy. In many cases, one is interested in processing a surface that has no residual stress prior to processing. In this case, $T'_d = 0$ and Eqs. (17-18) reduce to:

$$\theta''_{RS} = \frac{1}{2} \arctan\left(\frac{\beta_R C_P - \beta_P C_R}{\beta_R B_P - \beta_P B_R}\right), \qquad (24)$$

$$T''_d = \frac{\beta_R B_P - \beta_P B_R}{(\beta_R \varepsilon_P - \beta_P \varepsilon_R)\cos 2\theta''_{RS}}, \qquad (25)$$

$$T''_d = \frac{\beta_R C_P - \beta_P C_R}{(\beta_R \varepsilon_P - \beta_P \varepsilon_R)\sin 2\theta''_{RS}}. \qquad (26)$$

Eqs. (25) and (26) yield identical results. However, one or the other equation is ill-defined when θ''_{RS} is a multiple of $\pi/4$, in which case the other equation must be used. These equations state that the magnitude and direction of the residual stress anisotropy can be measured. Together Eq. (16) and Eqs. (24-26) describe entirely the residual stresses of the processed surface in terms of measurable parameters in the case where the initial residual stresses are zero. These equations are completely decoupled from texture modification that could arise at the surface from the LPB process. Note that only the 2θ dependence of the ultrasound velocity is required to characterize the residual stress anisotropy. However, the B and C parameters cannot be evaluated simultaneously without evaluating A and at least one of D, E, or some combination of D and E. Therefore, measurements at four different angles are necessary and sufficient to evaluate T''_m, T''_d, and θ''_{RS}. One such set of four measurements would be in the directions of $\theta = 0$, $\pi/4$, $\pi/2$, and $3\pi/4$.

As stated earlier, the texture symmetry direction of the surface before surface treatment is often known. For example, the rolling direction of rolled product is usually one such symmetry direction. In such cases, the reference angle for the ultrasonic and texture measurements can be taken as the rolling direction and $\theta'_w = 0$. This simplifies Eqs. (20-23) somewhat but still leaves 4 equations in 5 unknowns. However, if for metallurgical reasons it could be shown that the LPB process modifies surface texture in such a manner as to not affect the symmetry direction, then we would also have $\theta''_w = 0$. Possibly this could occur if the LPB process were applied in a specific direction. For example, the symmetry might not change if the rolling direction of the LPB process were the same as the rolling direction of a sheet product. If metallurgists could show this, then Eqs. (20-23) would reduce to two equations describing the texture changes $W''_{420} - W'_{420}$ and $W''_{440} - W'_{440}$.

Test sample

A square sample of 10.1 cm (4 inches) to a side was cut from a 22.2 mm (0.875 inch) thick commercial plate of aluminum alloy 7075-T651. This designation indicates that after being rolled, the plate was *solution heat treated and artificially aged* to improve mechanical properties and dimensional stability

[11]. The designation also indicates that following the heat treatment, the plate was *stress-relieved by stretching*, i.e. stretched a small amount, of order 1.5 to 3%, to flatten the plate and relieve residual stresses. Such stress relief procedures do not leave the plate residual stress free, but greatly reduce the magnitude of bulk residual stresses. Furthermore, the two faces of the plate were ground away using a low-stress grinding process. This process is known to leave anisotropic residual stresses of its own. These stresses are compressive and can be of fairly high magnitude with respect to the compressive yield stress of the alloy. However, they are typically only about 25 μm deep. Because ultrasonics probes depths of order 50 μm to a few mm, and because the penetration depth of the LPB process is of order 1 mm, the residual stresses induced by the low-stress grinding process will be assumed negligible. The final sample thickness was 20 mm and the surfaces were quite smooth.

The LPB process was applied to one half of one of the two surfaces. The exact process parameters are proprietary, but for the purpose of this paper, it is sufficient to know that the process produced a mirror-like surface quality. Also, x-ray measurements indicate that the surface residual stresses were respectively −187 ± 4 MPa and −423 ± 6 MPa in the direction of the LPB process and perpendicularly.

Ultrasonic Measurements and Data Analysis

Rayleigh and P waves, were measured using laser-ultrasonics. Laser-ultrasonics is a technology that generates and detects ultrasound using lasers. A general description of the technology and specific details regarding the measurement of Rayleigh and P waves can be found elsewhere [12,13]. The following operating parameters were utilized. The ultrasound source was a mode-locked laser, focused to a thin line 2 to 5 microns wide and approximately 5 mm long. The generation laser emitted ultraviolet (355 nm) pulses, 35 ps duration, and energy less than 1 mJ/pulse. Detection involved an infrared (1.06 μm) long-pulse laser of 50 μs pulse duration and an InPFe photorefractive interferometer [14]. Shutters limited the generation and detection repetition rates on the sample to 1 Hz to avoid heating the sample by the laser radiations and so obtain a velocity change caused by elastic constant variations with temperature. The detection radiation was also focused to a thin line approximately 2 mm long and approximately 20 μm thin. Adjustments were available to help make the source and detection lines parallel to each other, to control their separation, and to move and rotate the sample.

A schematics of the measurement geometry is shown in Fig. 1. The standard separation distance between the two lines was 4 mm. This distance was chosen because it was large enough to separate the Rayleigh and P waves and short enough to retain enough amplitude to measure the P wave with a good signal-to-noise ratio. Measurements were made as a function of angle with respect to the LPB processing direction, in steps of 15°, from 0 to 195°. In the 180° direction, measurements were also made in 1 mm increments, from 3 to 8 mm separation, to obtain the absolute sound velocity in that direction. The same procedure was applied on both an LPB-treated surface and on a non-treated surface of the same sample, approximately 5 cm away. It was assumed that the as-received surface texture and residual stresses did not vary significantly over such a short distance.

A typical ultrasonic signal displaying the time of arrival of the P pulse (near 0.6 μs) and Rayleigh pulse (near 1.2 μs) is shown in Fig. 2. The P-wave frequency content extends from 2 to about 15 MHz, while the Rayleigh wave frequency content extends from 2 to more that 60 MHz. The penetration depth of Rayleigh surface waves depends on wavelength or inverse frequency: the longer wavelengths (lower frequencies) penetrate deeper into the material [15]. Thus, the frequency information may provide information about depth dependence of stress and texture and it is of high interest. The relation between frequency and the penetration depth of P waves is currently an open question. Unfortunately, the frequency dependence is also affected by ultrasonic diffraction. In this paper, we shall compute this frequency dependence and use the information to insure that diffraction does not adversely affect the results. Further use of the frequency information is still under investigation.
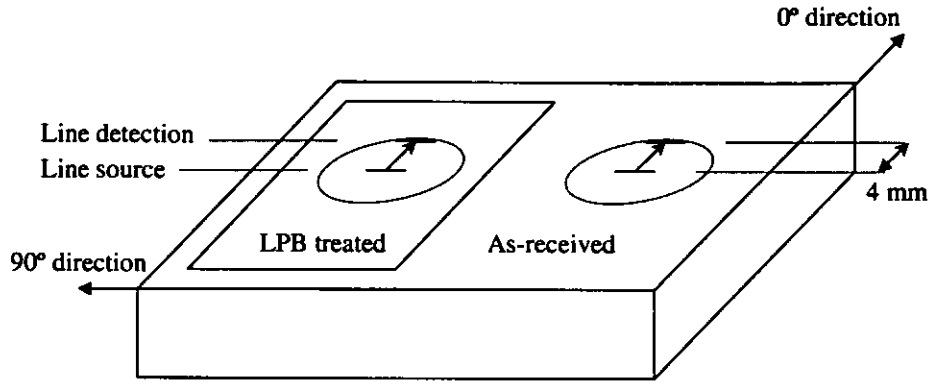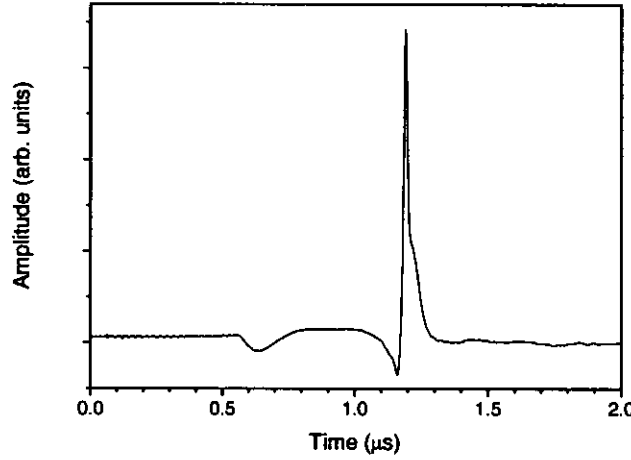
Figure 1: Schematics of the measurement setup.

Figure 2: Ultrasonic signal amplitude as a function of time. The P pulse arrives near 0.6 µs. The Rayleigh pulse arrives near 1.2 µs.

To obtain $\Delta V(\theta, f)/V_0$ from the data, the following analysis is made. First, the isotropic velocity is estimated from the propagation delay as a function of distance from the measurements taken in the 180° direction. For two propagation distances, x_1 and x_2, the Rayleigh or the P ultrasonic pulse is windowed and Fourier transformed, thus yielding an amplitude and phase for each frequency component. The phase difference between the two propagation distances is computed and converted to a propagation delay, $\Delta t(f)$. From this we estimate $V_0(f) = (x_2 - x_1)/ \Delta t(f)$. The result is shown in Fig. 3. The frequency dependence of the velocity is in large part due to ultrasonic diffraction. This is especially true at the low frequency end of the spectrum. Although this velocity spectrum depends on frequency and although it is obtained for a specific direction, V_0 will be chosen as some mean value of the frequency spectrum above 10 MHz where diffraction effects are less important. An error of a few percent on V_0 yields a systematic error of a few percent on the magnitude of the velocity variations, $\Delta V(\theta, f)/V_0$. This error is negligible.

The quantity $\Delta V(\theta, f)/V_0$ is obtained using a similar procedure. For each propagation direction θ, and for the two surfaces, the Rayleigh or the P ultrasonic pulse are windowed and Fourier transformed, thus yielding an amplitude and phase for each frequency component. The phase difference between the two surfaces is computed and converted to a propagation delay difference, Δt. In this case, diffraction effects largely cancel because the measurements are taken in the exact same geometry. The relative velocity variations are obtained by calculating

$$\frac{\Delta V}{V_0} = \frac{1}{V_0}\left(\frac{x}{t''} - \frac{x}{t'}\right) \approx -\frac{\Delta t}{t'} = -\frac{V_0 \Delta t}{x}, \tag{27}$$

where the prime and double prime refer to the as-received and LPB-treated surfaces, respectively, x is the 4 mm propagation distance, and $\Delta t = t'' - t'$. The results are shown in Figs. 4 and 5.
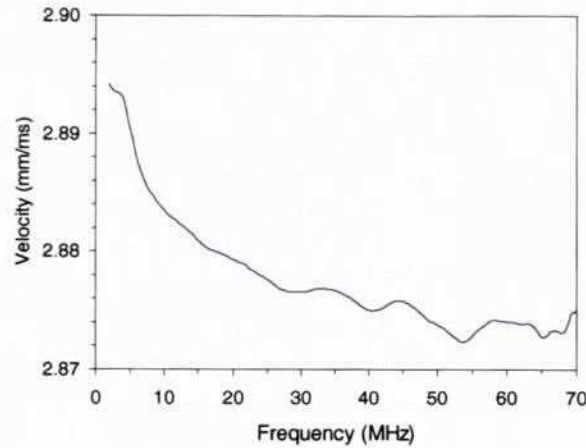

Figure 3: Ultrasound velocity in the rolling direction as a function of frequency. LPB-processed surface.
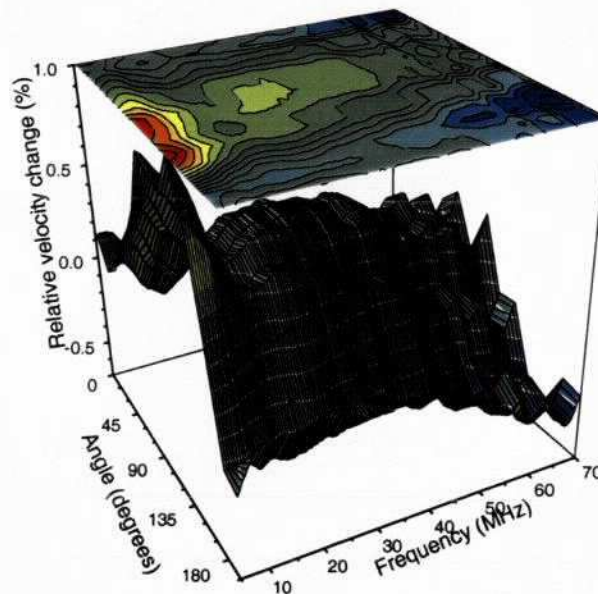

Figure 4: Relative change in Rayleigh wave velocity as a function of frequency and propagation angle. Each contour line represents a relative change of 0.1%.

The results show the following. Both the Rayleigh and P wave dependence show a relative velocity increase $\Delta V/V_0$ in the 90° direction (direction transverse to the LPB process). A detailed analysis shows that the frequency dependence of the P waves is not significant, i.e. it is due to measurement noise. However, the frequency dependence of the Rayleigh waves is significant. As mentioned earlier, the full analysis of the frequency dependence and its possible relationship to the depth dependence of the residual stresses is outside the scope of this paper. However, above approximately 20 MHz, the Rayleigh data is seen to be essentially independent of frequency. There are two reasons to expect this. First, diffraction effects are most important below 10 MHz and negligible at high frequencies. Second, at high enough frequencies, the waves are contained within the strained layer and do not penetrate into the bulk of the material. As an order of magnitude estimate, the wavelength and penetration depth of Rayleigh surface waves is approximately 100 μm at 30 MHz. As mentioned earlier, the penetration depth of P waves is an open problem. Here we will assume that P waves have the acoustic properties of the surface.
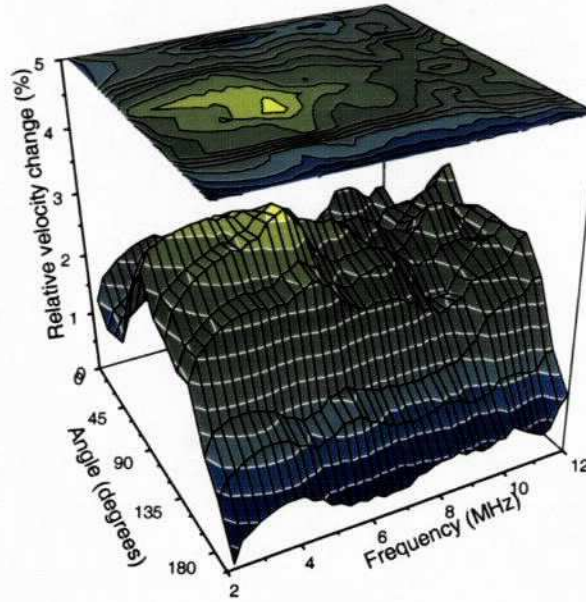
Figure 5: Relative change in P wave velocity as a function of frequency and propagation direction. Each contour line represents a relative change of 0.294%.

Taking into account the discussion of the preceding paragraph, and restricting our objective to the measurement of the residual stresses at the surface, $\Delta V/V_0$ will be taken as the average of the 20 to 60 MHz frequency components for the Rayleigh waves, and the average of the 3 to 12 MHz frequency components for the P waves. These are plotted and fitted to Eqs. (9-10) in Fig. 6. The fitted values are shown in Table I. The stated measurement errors are obtained from the statistical fitting procedure and are thus an estimate of reproducibility. For reasons that have to do with the ultrasound generation process [16] and that may be specific to the particular measurement configuration of this paper, the value of A_P suffers from an inaccuracy of order 10^{-2} that is not accounted for in the stated statistical errors. The measurement errors are smaller for the Rayleigh waves because these waves are measured with a better signal-to-noise ratio. However, the velocity variations of the P wave are larger and can tolerate a larger measurement error. Also, Fig. 6 shows that Rayleigh and P waves velocities have extrema at different angles. Substituting the fitted values of Table I into Eqs. (16) and (24-26) that are valid when the residual stress of the as-received surface is zero ($T'_m = T'_d = 0$), we obtain $\theta''_{RS} = 12.4°$, $\Delta T_m = T''_m = -498$ MPa, and $T''_d = -143$ MPa. Substitution into Eqs. (19-23) also shows that texture did change significantly as a result of the LPB process.

Discussion and Conclusion

The ultrasonically measured mean residual stress induced by the LPB process is compressive and equal to $T''_m = -498$ MPa. X-ray measurements of the surface residual stresses gave $T''_m = -305$ MPa. Although the agreement may seem poor at first, this is an excellent result. Referring to Eq. (16), we see that T''_m is highly sensitive to errors in A_P, a value that is relatively inaccurate. However, it is quite possible that future development in laser ultrasonic technology will provide a much more accurate value of A_P because the source of inaccuracy is now well understood as a result of this research work [16]. The result is also excellent because measurement involving Rayleigh waves have notoriously failed in the past. Most likely they have failed because they did not take into account texture changes near the surface. In contrast, our measurements are texture-independent.

The ultrasonic values of $\theta''_{RS} = 12.4°$ and $T''_d = -143$ MPa indicate that the residual stresses are anisotropic, that the principal axis of σ_a is 12° from the LPB rolling direction, which is also the plate

rolling direction. The measured value $(\sigma_2 - \sigma_1)/2 = -118$ MPa from x-rays is in general not equal to $T''_d = (\sigma_b - \sigma_a)/2$. The reason is that σ_2 and σ_1 are in the LPB-rolling and transverse direction. The ultrasonic measurements indicate that the principal stresses are 12° away from those directions. If the ultrasonic data is to be compared with x-rays, we calculate from the ultrasonic data that $(\sigma_2 - \sigma_1)/2 = \frac{1}{2} (\sigma_b - \sigma_a) \cos 2\theta''_{RS} = -130$ MPa. With this value, x-ray and ultrasonics agree within approximately 10%. This result is independent of texture and of texture modifications that the LPB process would have caused and that the ultrasound appears to have sensed. This result was obtained within the relatively general assumption that that the overall texture anisotropy is orthorhombic with one axis of symmetry being perpendicular to the surface normal. No assumption was made regarding the orientation of the symmetry axes in the plane of the plate. These measurements of θ''_{RS} and T''_d represent further improvements over the usual ultrasonic measurements.

The x-ray results provided here are surface measurements of residual stresses on the treated surface only. More detailed x-ray measurements of residual stresses and texture as a function of depth are planned. Also, the frequency information of the ultrasonic measurements has not yet been utilized to characterize the depth profile. Once both the x-ray and ultrasonic analyses are fully completed, a more accurate comparison of x-ray and ultrasonic capabilities will be possible.
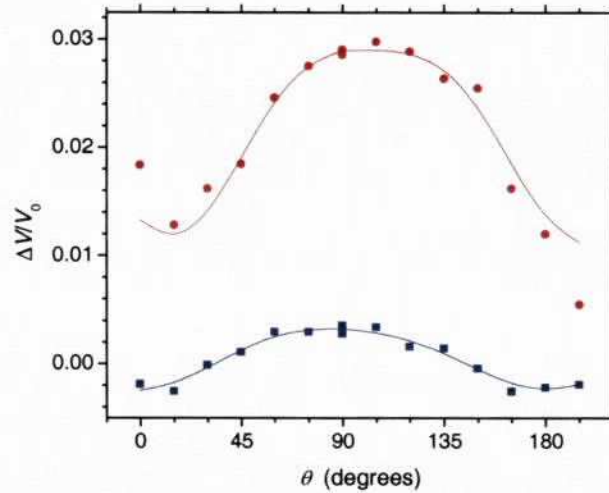

Figure 6: Blue square symbols and line: Angular variation of $\Delta V_R/V_{R0}$ in the frequency bandwidth of 20 to 60 MHz. Red circular symbols and line: Angular variation of $\Delta V_P/V_{P0}$ in the frequency bandwidth of 3 to 12 MHz. The symbols are the experimental data and the lines pertain to the fitted model.

Table I. Parameters of Eqs. (9-10) fitted to the experimental results of Fig. (6). The statistical errors are approximately ± 0.02 % for Rayleigh waves, and ± 0.1 % for P waves.

	A	B	C	D	E
Rayleigh Wave	0.075 %	–0.286 %	0.015 %	–0.039 %	–0.008 %
P wave	2.2 %	–0.78 %	–0.42 %	–0.11 %	–0.17 %

Acknowledgement

REFERENCES

1   M. P. Blodgett and P. B. Nagy, "On the Feasibility of Eddy Current Characterization of the Near-Surface Residual Stress Distribution in Nickel-Base Superalloys" *Rev. of Prog. in Quant. Nondest. Eval.*, 23B, D. O. Thompson and D. E. Chimenti, eds. (Melville NY, Am. Inst. of Phys., 2004), 1216–1223.

2.   C.-S. Man, "Hartig's Law and Linear Elasticity with Initial Stress" *Inverse Problems*, 14 (1998), 313–319.

3.   C.-S. Man and W. Y. Lu, "Towards an Acoustoelastic Theory for Measurement of Residual Stress" *J. Elasticity*, 17 (1987), 159–182.

4.   M. Huang and C.-S. Man, "Constitutive Relation of Elastic Polycrystal with Quadratic Texture Dependence" *J. Elasticity*, 72 (2003), 183–212.

5.   C.-S. Man and R. Paroni, "On the Separation of Stress-Induced and Texture-Induced Birefringence in Acoustoelasticity" *J. Elasticity*, 45 (1996), 91–116.

6.   R. Paroni and C.-S. Man, "Two Micromechanical Models in Acoustoelasticity: a Comparative Study" *J. Elasticity*, 59 (2000), 145–173.

7.   J. F. Thomas, "Third Order Elastic Constants of Aluminum" *Phys. Rev.*, 175 (1968), 955–962.

8.   V. Sarma and P. Reddy, "Third Order Elastic Constants of Aluminum" *Phys. Stat. Sol. A*, 10 (1972), 563–567.

9.   R.-J. Roe. "Description of Crystallite Orientation in Polycrystalline Materials. III. General Solution to Pole Figure Inversion" *J. Appl. Phys.*, 36 (6) (1965), 2024–2031.

10. H.-J. Bunge, *Texture Analysis in Materials Science* (London, Butterworths, 1982).

11. H. E. Boyer and T. L. Gall, eds., *Metals Handbook Desk Edition* (Metals Park OH, American Society for Metals, 1985).

12. B. Chenni, A. Moreau and J. Pouliquen, "NDE of Zinc Layer on Steel Substrate Using Laser-Ultrasonic SAW" *Proc. SPIE Conf. on NDE for Health Monitoring and Diagnostics – Nondest. Eval. & Reliability of Micro and Nanomaterial Systems.* (SPIE The Internat. Soc. for Opt. Eng., 2002) 14–20.

13. C. Bescond et al., "Determination of residual stresses using laser-generated surface skimming longitudinal waves" *Proc. SPIE Vol. 5767, Nondestr. Eval. and Health Monitoring of Aerospace Materials, Composites, and Civil Infrastructure IV*. P. J. Shull, A. L. Gyekenyesi and A. A. Mufti, eds. (SPIE The Internat. Soc. for Opt. Eng., 2005) 175-186.

14. P. Delaye et al., "Detection of ultrasonic motion of a scattering surface using photorefractive InP:Fe under applied DC field" *J. Optical Soc. of Am.*, B (14) (1997), 1–12.

15. B. A. Auld, *Acoustic Fields and Waves in Solids* 2nd ed. (Malabar FL, Krieger, 1990), Vol II, p. 92.

16. A. Moreau, *unpublished.*